Mass Measurements of a Heavy Neutralino Signal in an NLC Detector

Dave Staszak

July 24, 2003

Abstract

This paper investigates the feasibility of measuring the masses of two Supersymmetric particles at the proposed Next Linear Collider (NLC). Supersymmetry (SUSY) is a theorized extension to the Standard Model of Particle Physics. Precise measurements of SUSY's characteristics, such as particle masses and cross sections, will require an electron-positron accelerator like the NLC. In this study, the procedure for measuring the masses of two of the heaviest and rarest predicted Supersymmetric particles, the $\widetilde{\chi}_3^0$ and the $\widetilde{\chi}_4^0$, is outlined. Three cuts were devised that eliminated 99.99% of the background events while retaining 58% of the original signal events. The Energy Endpoint Method was used for a particular reaction mode to arrive at equations explicitly solving for the masses of the $\widetilde{\chi}_3^0$ and $\widetilde{\chi}_4^0$ dependent only on M_Z, $M_{\widetilde{\chi}_1^0}$, and the two Z^0 energy endpoints. These masses were successfully measured to $\sim$ 10 GeV resolution after two assumptions were made. First, that the mass of a lighter Supersymmetric particle, the $\widetilde{\chi}_1^0$, has already been measured, and second, that the Vertex Detector in the NLC has a spatial resolution of at least 20 μm.

Contents

1 Introduction

Supersymmetric particles have been studied in a simulated Next Linear Collider (NLC) by our research group and others. The purpose of these simulations is to investigate the feasibility of measuring particular characteristics of Supersymmetry, such as a Supersymmetric particle's mass or cross section, in an accelerator and detector that is still in the design phase. This information is important as the High Energy Physics community begins to finalize designs of this NLC. The Supersymmetric signal, or particular type of event, that was focused on in this paper was $e^+e^- \to \tilde{\chi}_3^0\tilde{\chi}_4^0$. This project is important in this regard, as none of the prior studies looked at a signal that is as heavy and rare as this one. If Supersymmetry is shown to exist in nature as an extension to the current Standard Model of Particle Physics, physicists will want to measure all of its characteristics, not just the easy ones. Results of this study show that measuring Supersymmetric signals like this one is more involved, but possible at the NLC.

In this study, the Energy Endpoint Method was used to measure the masses of the $\tilde{\chi}_3^0$ and $\tilde{\chi}_4^0$ Supersymmetric particles. To use this endpoint method, the energy of a resulting particle that one of these Supersymmetric particles decays into must be resolved and measured. It was necessary to isolate specific decay channels for each of these Supersymmetric particles to find the resulting particle's energy. There are a few problems that arise during this process. First, when isolating particular decay channels for each of these particles,one is only able to look at a portion of the total amount of $e^+e^- \to \tilde{\chi}_3^0\tilde{\chi}_4^0$ events that occur in a set time. A problem with statistics naturally arises that is only solved by looking at a larger time period of simulated data. Second, there are numerous other Supersymmetric processes, or signals, that the e^+ and e^- annihilate into within a time period. These background events are in the way as one tries to isolate the particular channels studied. Methods need to be developed and implemented that remove substantial numbers of these events while keeping the signal events intact. These procedures and problems will constitute a substantial amount of the analysis found in this paper.

Before discussing the assumptions and procedures in this study, a brief discussion of the Physics behind the project is necessary.

2 The Standard Model and Supersymmetry

2.1 The Standard Model of Particle Physics

Current understanding of the most fundamental level of particle interactions is explained in the Standard Model of Particle Physics. The Standard Model classifies all elementary particles as one of two types, either a fermion or a boson. Fermions are particles which are the building blocks for all visible particles and matter and have half integer spin quantum numbers[1]. Bosons are particles that carry the forces exchanged between two interacting particles and have integer spins. Understanding the characteristics of fermions and bosons is crucial to this study.

Fermions: Spin Quantum Number: $\frac{1}{2}\hbar$

Generation	Leptons	Quarks
1	e ν_e	d u
2	μ ν_μ	s c
3	τ ν_τ	b t

Bosons: Spin Quantum Number: $1\hbar$

Force	Particle	Name
Electromagnetic	γ	*Photon*
Weak	$W^\pm, Z^0$	*Weak Bosons*
Strong	g	*Gluon*

Table 1: The fundamental particles in the Standard Model.

The fundamental particles in the Standard Model can be seen in Table 1. Table 1 was in a sense completed in 1995, when the top quark (t) was finally discovered at Fermilab. This table is intended to show the fundamental particles that make up the Standard Model, but by no means are these the only particles found in nature. The particles in this table represent the lowest level of structure that we have evidence of. Many theories of further

[1]Spin is a measurement of the intrinsic angular momentum of particles. The spin quantum number s is a half integer or integer number while the spin is given as $\sqrt{s(s+1)}\hbar$. I am going to use spin and spin quantum number somewhat synonymously in this paper.

underlying structure have been postulated, but no evidence has been found yet. There are many additional fermions and bosons that have been seen experimentally made from combinations of these fundamental fermions. In the case that these additional higher mass particles are made out of quark anti-quark pairs or three quarks, we call these particles hadrons.

In Table 1, fermions are subdivided into six quarks and six leptons. Of these, the electron (e^-), the up quark (u), and the down quark (d) are what make up most of the matter that is stable and seen in the universe. For instance, the proton is made up of two up quarks and one down quark, and the neutron consists of two down quarks and one up quark. As the generation of any particular fundamental fermion goes up, as referenced in Table 1, so does its mass. The more massive a particle, the less stable. So while electrons and muons ($\mu^\pm$) are fairly easy to see in a detector, the tau ($\tau^\pm$) is so unstable that it decays about 100 μm from where it is produced and can only be seen in the detector through its decay products[2]. It is one of the most interesting unanswered questions in physics today why nature exhibits this generation structure.

Every fermion in this table has an anti-partner with the opposite charge but the same mass. For the electron e^-, this is the positron e^+, for the muon μ^-, the anti-muon μ^+. Even the chargeless neutrinos have anti-partners, ν_e and $\overline{\nu_e}$. These neutrinos, which come in each of the three lepton flavors, are leptons that only interact weakly with matter. For the purposes of this study, this means that neutrinos don't interact with the detector and are essentially invisible.

The fundamental bosons are subdivided according to which of the four forces that boson carries; the Electromagnetic, the Strong Nuclear, the Weak Nuclear, or the Gravitational force[3]. The boson theorized to carry the Gravitational force, the graviton, has yet to be discovered and is not a part of the Standard Model.

To illustrate the role of these bosons, what keeps a neutron (udd) together is the Strong Nuclear force. This is mediated by gluons interacting between the quarks, keeping them within a metaphorical 'neutron bag'. When one of the down quarks in this neutron decays to an up quark though, a weak interaction has occurred, a decay. Nuclear physicists call this process beta

[2]The μ is known to have a mass on the order of 105 MeV/c^2, while the τ has a mass of $1777 MeV/c^2$, a full order of magnitude higher.

[3]We also like to think of these as the four fundamental fields in nature.

decay because an e^- and an $\overline{\nu_e}$ are released, and the neutron has effectively become a proton. In this case, the weak decay is mediated by the W^- boson.

There is one more boson that is predicted by the Standard Model that has yet to be found. The Higgs boson, h^0, is critical to this particular study and to Supersymmetry in general. The h^0 is the boson theorized to give rise to the mass of all the other particles. Particles interact with the h^0. The stronger their interaction is with the h^0, the more massive that particle is. For example, the τ is an order of magnitude more massive that the μ, so the τ interacts, or couples, much stronger with the h^0 than the μ. Physicists have been searching for this particle in colliders for many years now, and it is generally thought that more collision interaction energy is required to produce these particles frequently enough for people to see them. This is one of the main cases for larger colliders with increased energy.

2.2 Problems in the Standard Model

The Standard Model, through the experimental tests of roughly twenty years, has proven to be a very sound description of the interactions of the known elementary particles. As the theory is understood today though, there are still a few holes or difficulties in our overall understanding of how and why things work the way they do.

One such difficulty, as briefly mentioned in Section 2.1 above, is that the nature of mass in the Standard Model is an unexplained phenomenon. It is not understood why the electron, the muon, and the tau, which all exhibit nearly identical characteristics, have different masses. What is the nature of this mass, and where does it come from? The h^0 is a theorized boson that represents the first step towards understanding this phenomenon. The h^0, if it exists, explains at least where this mass comes from. There is a problem with the h^0 as predicted by the Standard Model though. When the mass of the h^0 is calculated, it is infinite. With the addition of Supersymmetry, which I will talk about in greater length below, this mass becomes finite.

Since Einstein's time, physicists have been searching for the theory that unites all theories, the so-called Grand Unification Theory (GUT). While progress has been made towards this end, a unified theory has not been realized. The Electromagnetic and Weak forces were experimentally shown to be equal at energies around 80-90 GeV by the early 80's. What resulted was known as Electroweak Theory. Efforts to combine the Gravitational forces with the Standard Model forces (the Electroweak and Strong) have not yielded any tangible evidence, and the Electroweak and Strong forces do not converge under the current theoretical predictions of the Standard Model. Supersymmetric extensions to the Standard Model help toward this end by predicting a converge of these Standard Model forces at high energies.

2.3 Supersymmetric Extensions to the Standard Model

Supersymmetry (SUSY) is a theoretical extension of the Standard Model. Supersymmetry predicts two new Higgs doublets and a partner particle opposite every known particle with a spin quantum number that is a half integer off the Standard Model particles in Table 1. Therefore, the Supersymmetric partner of a boson is a fermion and vice versa.

Sparticles: 'Scalar Particles'

Standard Model	Supersymmetry
$e^{\pm}$	$\widetilde{e}^{\pm}_L$, $\widetilde{e}^{\pm}_R$
$\mu^{\pm}$	$\widetilde{\mu}^{\pm}_L$, $\widetilde{\mu}^{\pm}_R$
$\tau^{\pm}$	$\widetilde{\tau}^{\pm}_1$, $\widetilde{\tau}^{\pm}_2$
$\nu_{e,\mu,\tau}$	$\widetilde{\nu}_{e,\mu,\tau}$
u, d	$\widetilde{u}_L$, $\widetilde{u}_R$, $\widetilde{d}_L$, $\widetilde{d}_R$
c, s	$\widetilde{c}_L$, $\widetilde{c}_R$, $\widetilde{s}_L$, $\widetilde{s}_R$
t, b	$\widetilde{t}_L$, $\widetilde{t}_R$, $\widetilde{b}_L$, $\widetilde{b}_R$

Gauginos and Higgsinos

Standard Model	Supersymmetry
g	$\widetilde{g}$
$W^{\pm}$, $H^{\pm}$	$\widetilde{\chi}^{\pm}_1$, $\widetilde{\chi}^{\pm}_2$
γ, Z^0, h^0, H^0	$\widetilde{\chi}^0_1$, $\widetilde{\chi}^0_2$, $\widetilde{\chi}^0_3$, $\widetilde{\chi}^0_4$

Table 2: The additional Supersymmetric partner particles introduced. The two blue particles are new Standard Model particles introduced by Supersymmetry. They are labeled Standard Model because of their spin characteristics. The two red particles are those that I am studying in this paper.

As seen in Table 2, there is a Supersymmetric partner assigned to every Standard Model particle. An electron can have both right-handed and left-handed helicity[4], so there is a Supersymmetric selectron ($\tilde{e}_L^{\pm}$, $\tilde{e}_R^{\pm}$) associated with each of these cases. The nomenclature taken for these Supersymmetric particles is also shown in Table 2. The Supersymmetric partner of a fermion is called a sfermion, or a scalar fermion, and likewise the partner of a quark is a squark. The idea of a scalar particle is a direct analogy to vector quantities: a spin 0 particle is known as a scalar particle, while a spin 1 particle is a called a vector particle. For bosons, the Supersymmetric partners are fermions and the nomenclature is slightly different, but just as straight-forward. The Supersymmetric partner is the name of the boson with an 'ino' suffix.

As mentioned above, Supersymmetry is a very appealing addition to the Standard Model for a number of theoretical reasons. First, Supersymmetry predicts a finite mass h^0. Due to Heisenberg Uncertainty ($\Delta E \Delta t \sim \hbar$), in an extremely short timescale energy fluctuations will allow the h^0 to temporarily dissociate into any particle anti-particle pair. Each of these possible dissociations gives a correcting term in the theoretical calculation of the h^0's mass. With Standard Model particles alone, this leads to an infinite h^0 mass. However, when Supersymmetric particles are included, SUSY yields additional correcting terms to the present correcting terms. It turns out that Supersymmetric terms cancel out Standard Model terms, and what results is a finite h^0.

Second, Supersymmetry also provides very important implications in the pursuit of the GUT discussed above. SUSY causes the coupling constants[5] of the three fundamental forces to converge at very high energies, around 10^{16} GeV, effectively combining them into one[1][2]. This is an exciting conclusion that has been sought for many years. The dependence of these coupling constants on the interaction energy can be seen in Figures 1 and 2.

---

[4] Helicity is a measure of the momentum of a particle relative to the direction of its intrinsic spin. A right-handed particle has momentum in the same direction as its spin (right-hand rule).

[5] Examples of coupling constants are G in Newtonian gravity and $\alpha = \frac{e^2}{\hbar c}$ in electromagnetism. A coupling constant describes the strength of the interaction between two particles under some field. Obviously, coupling constants are not precisely constants in nature as seen in Figures 1 and 2. It has been shown experimentally that coupling constants are affected by the interaction energy. For example, the coupling constant α above is $\frac{1}{137}$ at low energies and $\frac{1}{127}$ at energies around the electroweak scale $\sim$ 80-90 GeV.

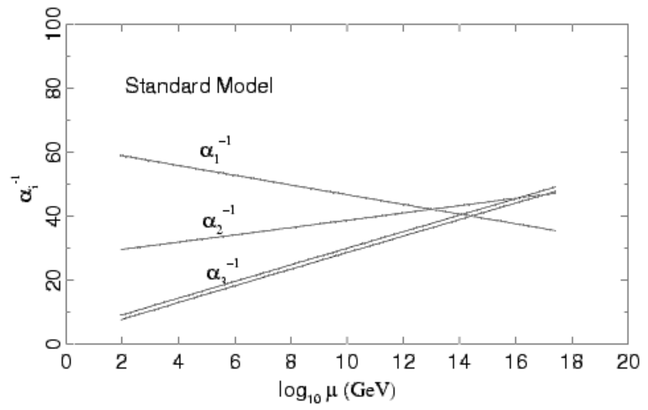

Figure 1: Plot of the inverse coupling constants of two of the three fundamental forces with only Standard Model particles. Combinations of α_1 and α_2 represent the Electroweak coupling constants. α_3 is the inverse coupling constant for the Strong force with 2 lines representing an uncertainty.

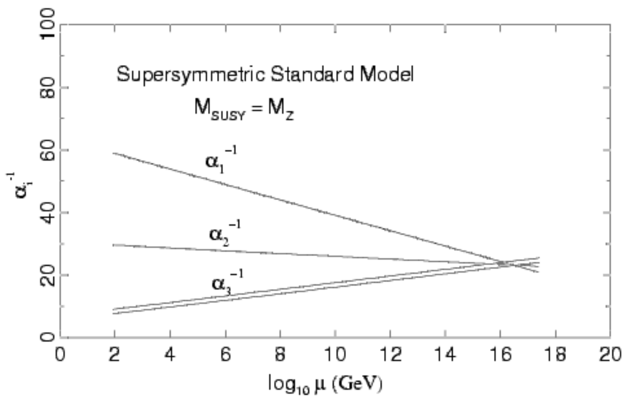

Figure 2: The inverse coupling constants with Supersymmetric and Standard Model particles. $M_{SUSY} = M_Z$ refers to the prediction of the masses of Supersymmetric particles to be on the order of the Z boson mass. The dependence of these coupling constants is logarithmic with mass, so this prediction is roughly anywhere from 90 GeV/c^2 to 900 GeV/c^2.

3 The Next Linear Collider

3.1 Motivations for the NLC

High Energy Physics is a collaborative undertaking. This is because to probe the unknown in High Energy Physics requires gigantic machines that cost billions of dollars. The case for a new, higher energy linear collider is now being made across the globe. Three major designs have been developed worldwide for this future linear collider, the Next Linear Collider (NLC) in America, the Japanese Linear Collider (JLC) in Japan, and the Tera Electron Volt Energy Superconducting Linear Accelerator (TESLA) in Europe. Primarily for funding reasons, one design will be selected by everyone involved so that production can start ideally in the next decade.

If selected, the NLC will be an electron-positron collider with a collision interaction energy starting at 500 GeV with upgrades planned to reach as high as 1.5 TeV. A schematic for the NLC can be seen in Appendix A. The current interaction energy that has been successfully probed worldwide reaches as high as ~ 200 GeV. In this energy region searched to date, no evidence for SUSY has yet been found, and no conclusive evidence of the h^0 has either. The NLC is desired in order to push this energy frontier further.

Data analysis for the Tevatron collider at Fermilab is currently starting to be published, but the interaction energy there is only slightly higher than 200 GeV. Additionally, in Europe, the Large Hadronic Collider (LHC) is in the early stages of construction. This LHC will probe the same energy region as the NLC. While the LHC or the Tevatron could very well discover the h^0, they will not be able to tell us all the details of SUSY. Both of these machines are proton-antiproton accelerators, and they will not be able to measure all of the precise parameters of Supersymmetry that the NLC will. For this reason, the LHC and NLC are thought of as complimentary in this energy region. It is much easier to make a higher energy proton-antiproton accelerator, but because these collided particles interact mainly through strong processes, each event will be filled with potentially hundreds of particles that will clutter precise measurements[6]. To make precise measurements of the SUSY interaction characteristics, electron-positron accelerators provide reactions that are relatively clean, with few visible particles, that will allow measurements of

[6] The LHC is designed to be a 7 TeV accelerator. Proton-antiproton collisions result in the interaction of two quarks though, so the interaction energy is roughly 1/9 of the total interaction energy. The interaction of these two quarks causes strong processes.

cross-sections and masses to be made with extreme accuracy.

3.2 The Detector

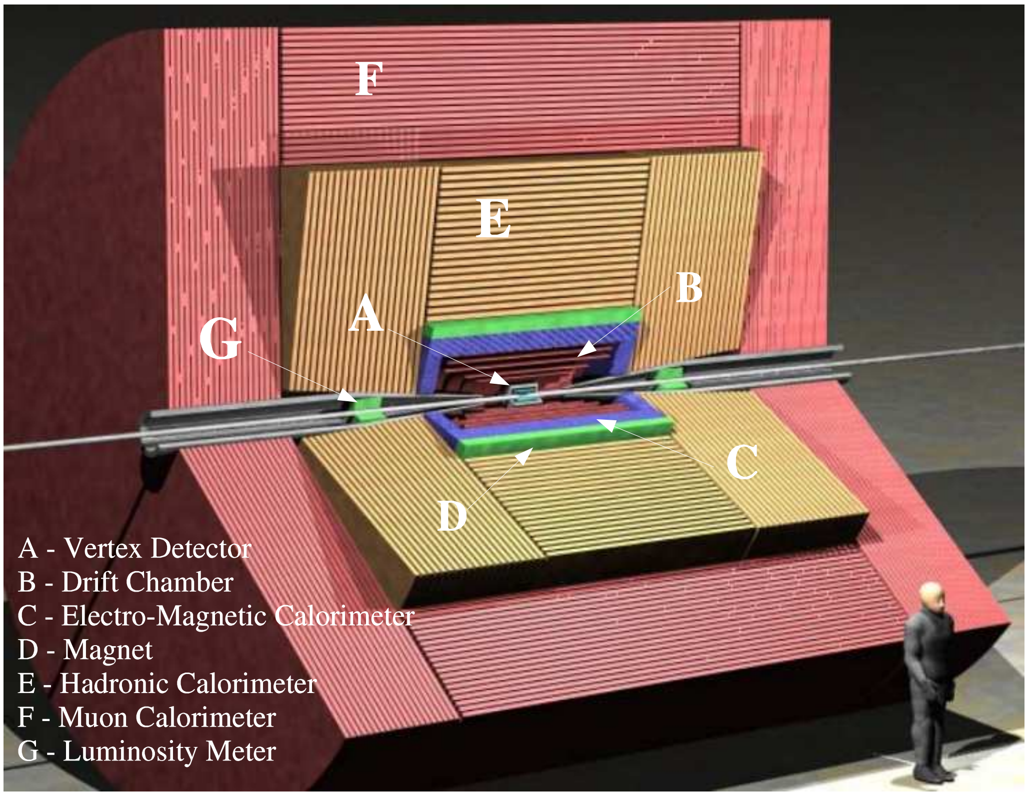

Figure 3: Schematic of the NLC's Detector

Figure 3 shows a rough schematic of the NLC's detector. Since this detector is at least a decade away from production, it has to be simulated. There are various programs used by my research group to model the effects of this detector.

Referring to Figure 3, just outside of the interaction point of the electron and positron beams is what is called the Vertex Detector (labeled A in figure). This is a very important part of the detector for this particular study. The purpose of the Vertex Detector is to be able to identify decay vertices that are separate from the main vertex (interaction point). To illustrate this assume, on average, that the τ decays 87.11 μm from the point that it was produced. Take the case that a particular τ, after flying through 87.11 μm of the Vertex Detector, then decays into a single lepton. The Vertex Detector is able to reconstruct where the particular decay vertex of this τ was from information gathered about the lepton. This procedure is used to label the initial unseen particle as a τ. If a single lepton track begins about 80 μm from the central vertex, it can be reasonably said it came from a τ.

The next portion of the detector, labeled B, is called the Drift Chamber. The Drift Chamber is filled with a gas such that charged particles traveling through it leave a trail (or track) of ionized gas particles in their wake. The Drift Chamber is used to measure a particle's curvature (and thus momentum) as it travels through that portion of the detector. A magnet, here labeled D, is the mechanism that causes charged particle's trajectories to curve.

Section C is called the Electromagnetic Calorimeter. The Electromagnetic Calorimeter is made of alternating layers of a heavy charged atomic material, a light sensitive material (like scintillator), and is used primarily to measure electrons and photons. Electrons entering the EM Calorimeter interact with the heavy atom's electric field by exchanging a virtual γ. This process produces an additional electron-positron pair which then interacts in the same way, and starts a cascading shower of energy that the calorimeter measures. Photons will interact in a similar manner.

Part E is the Hadronic Calorimeter. The Hadronic Calorimeter is mainly used to measure the kinetic energy of neutral particles, specifically the K_L^0 (K Long) and the neutron. F represents the Muon Calorimeter and is almost exclusively used to identify and measure Muons in the detector. The last portion, the Luminosity Meter (labeled G), is used to measure the luminosity of the beam. Work has been done by our research group on a Cerenkov Detector that would be placed in the inner ring of this Luminosity meter[3] [4].

4 Experimental Methodology

4.1 Simulating the NLC

Performing this research requires the simulation of the necessary collisions and decays, as well as the response of the detector to them. Three main programs were used to perform these simulations. The first was a program written at Brookhaven National Laboratory called ISAJET[5] that generates all the particle decays from the initial e^+ and e^- to the final stable decay products. This program simulates known physical processes as well as unknown physical processes, like those that occur in SUSY. Since the characteristics of SUSY are not known, theorists have identified numerous potential versions of SUSY. Each of these versions can be simulated with ISAJET. Our group looks at variations of the MSSM, or Minimum Supersymmetric Standard Model, a model that calls for the minimum amount of change from the Standard Model. The particular form of the MSSM studied here is called the mSUGRA model, or the minimum supergravity model. For this mSUGRA version of SUSY, there are four main parameters that theorists have identified as vital to where and how SUSY resides, they are[6]:

- m_0 universal scalar mass
- $m_{1/2}$ universal gaugino mass
- μ Supersymmetric Higgsino mass parameter
- $\tan\beta$ ratio of the vacuum expectation values of the two neutral Higgs scalars

Theorists have identified certain benchmarks, or parameter space points, that represent versions of potential Supersymmetry based on these parameters. Each of these points determine sparticle masses, branching ratios, and cross sections for Supersymmetric signals[7]. Using benchmarks chosen at Snowmass 2001 as a guide[8], my research group chose to investigate one of these mSUGRA parameter points that looked particularly messy, with many hadronic and τ decays. This particular point, SPS 1, one of nine parameter points that were introduced at this conference, has the following values for the above parameters:

- $m_0 = 100\ GeV/c^2$
- $m_{1/2} = 250\ GeV/c^2$
- $\mu = 352.39\ GeV/c^2$

[7]Cross sections are a measure of how frequently a process occurs at a given luminosity. Branching ratios tell you how frequently particular decay channels of particles occur.

	minimal SUGRA						GMSB		AMSB
	SPS1	SPS2	SPS3	SPS4	SPS5	SPS6	SPS7	SPS8	SPS9
$\widetilde{\chi}_1^0$	96.1	79.5	160.6	118.7	119.5	175.5	117.5	161.7	137.2
$\widetilde{\chi}_2^0$	176.8	135.3	297.0	218.1	226.3	549.0	215.5	260.1	252.3
$\widetilde{\chi}_3^0$	358.8	140.8	512.9	383.9	642.8	874.4	398.7	306.3	404.0
$\widetilde{\chi}_4^0$	377.8	269.5	529.6	401.1	653.0	876.0	418.1	379.9	426.3
$\widetilde{\chi}_1^+$	96.1	79.5	160.6	118.7	119.5	175.5	117.5	161.7	137.2
$\widetilde{\chi}_2^+$	176.8	135.3	297.0	218.1	226.3	549.0	215.5	260.1	252.3
h^0	114.0	115.7	117.0	115.4	119.8	114.8	114.7	113.6	114.8
H^0	394.2	1444.1	573.0	404.6	694.0	912.6	457.8	378.4	515.0
A^0	393.6	1443.0	572.4	404.4	693.9	911.7	457.3	377.9	514.5
H^+	401.8	1446.2	578.3	416.3	698.5	915.8	464.4	386.7	521.2
$\widetilde{\nu}_e$	186.0	1454.2	276.0	441.2	244.5	309.7	243.3	249.1	347.6
$\widetilde{e}_R^-$	143.0	1451.7	178.3	416.5	191.5	303.0	191.3	127.4	175.9
$\widetilde{e}_L^-$	202.1	1456.3	287.1	448.4	256.3	319.7	255.8	261.5	356.6
$\widetilde{\tau}_1^-$	133.2	1439.5	170.6	267.6	180.7	271.3	184.3	120.5	169.4
$\widetilde{\tau}_2^-$	206.1	1450.4	289.2	414.9	257.9	322.5	258.3	263.4	357.6
$\widetilde{t}_1$	379.1	1003.9	623.8	530.6	220.7	1005.2	474.1	779.1	957.7
$\widetilde{t}_2$	574.7	1307.4	819.5	695.9	644.7	1128.8	659.7	863.0	1058.7
$\widetilde{b}_1$	491.9	1296.6	757.5	606.9	535.9	1112.1	589.8	822.2	1021.9
$\widetilde{b}_2$	524.6	1520.1	791.4	706.5	623.0	1232.9	623.4	843.4	1048.3
$\widetilde{u}_R$	520.5	1530.1	791.8	715.1	624.5	1227.4	621.9	830.5	1033.2
$\widetilde{u}_L$	537.3	1532.7	816.6	730.2	641.8	1218.1	639.0	859.7	1080.3
$\widetilde{g}$	595.2	784.4	914.3	721.0	710.3	1275.2	708.6	926.0	820.5

Table 3: Mass spectrum for nine SUSY parameter points.

- $\tan\beta = 10$

Table 3 shows the masses that these parameter values predict along with the other eight possible versions.

Knowing this, ISAJET can generate all of the Supersymmetric processes that will occur in a specified time of simulated data collection at the NLC. All initial radiation processes, such as beamstrahlung and bremsstrahlung have been included. ISAJET was run at at an interaction energy of 750 GeV, which, as can be seen in Table 3, is right above the production threshold for the $\widetilde{\chi}_3^0\widetilde{\chi}_4^0$ signal. Additionally, the luminosity used was 500 fb^{-1}, and 10 years worth of data was generated for statistics.

After all the physical processes have been simulated by ISAJET in their ideal form, the next step is to add in the effect of the detector. This step simulates what would actually be seen and measured in each event. NLCPROC is used to include this effect. The program is what is called a fast simulation because it does not go through the detector layers step by step to add in each layer's response. Rather, it uses an energy smearing algorithm on all of the final decay products that mimics what the detector would see.

The third and last program used is a program written at CERN called ROOT and is a data analysis program. Inputting all of the data from ISAJET and NLCPROC into ROOT, I can write code in C and C++ to perform analysis on it.

4.2 The Energy Endpoint Method

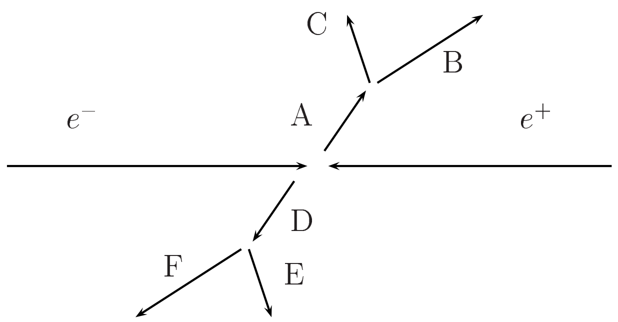

The Endpoint Method was originally devised by Tsukamoto et al.[6]. It is a method that is based on energy endpoints that come from Lorentz boosting a decay particle out of the center of mass frame of its parent particle. In the schematic shown above, particle C's lab energy (the energy in the detector's frame of reference) depends directly on particle A's Lorentz boost given by the relativistic equation:

$$E_C^{LAB} = \gamma_A(E_C^{CM} + \beta_A P_C^{CM} cos\theta)$$

The cosine term in this expression will create two physical energy endpoints for particle C. These endpoints depend on what direction particle C is moving in particle A's center of mass frame with respect to particle A's Lorentz boost. Figure 4 shows this box distribution, where the flat top comes from the fact that all the values of cosine from -1 to 1 in the above equation are equally probable.

Using these two endpoints as measurable quantities will allow for the measurement of the masses of particles A and D. With $\tilde{\chi}_3^0$ as particle A above, $\tilde{\chi}_4^0$ as particle D, Z^0 as particle C, and $\tilde{\chi}_1^0$ as particle B, we can solve for Equations 1 and 2. See Appendix B for the full derivation of these equations. One important assumption needs to be made. The mass of the $\tilde{\chi}_1^0$ has to already be measured. This is a valid assumption to make because the signal studied here is one of the heaviest of all (Table 3), and will therefore be one of the last to be measured. There are many signals, such as sleptons, which are much cleaner and lighter, that will be measured before this one, and which lead directly to mass measurements of the $\tilde{\chi}_1^0$ [10]. So, with $\sqrt{s}$ as the accelerator interaction energy and E_Z^{HI} and E_Z^{LOW} as the respective energy endpoints of the Z^0, the equations for the masses of the $\tilde{\chi}_3^0$ and $\tilde{\chi}_4^0$ are:

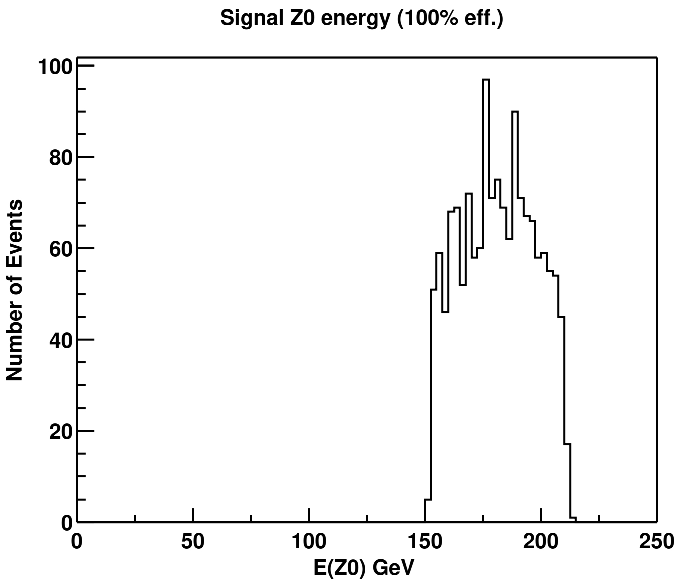

Figure 4: Box energy distribution of the Z^0 (particle C) coming from $\tilde{\chi}_3^0$ (particle A) decays.

$$M_{\tilde{\chi}_3^0} = d + \sqrt{d^2 - ({M_Z}^2 - {M_{\tilde{\chi}_1^0}}^2)} \tag{1}$$

with

$$d^2 = \frac{(E_Z^{LOW} * E_Z^{HI} + M_Z^2)}{2} + \frac{\sqrt{(E_Z^{LOW} * E_Z^{HI} + M_Z^2)^2 - M_Z^2 * (E_Z^{LOW} + E_Z^{HI})^2}}{2}$$

and we can also get:

$$M_{\tilde{\chi}_4^0} = \sqrt{M_{\tilde{\chi}_3^0}^2 + s - \sqrt{s} * (E_Z^{LOW} + E_Z^{HI}) * \frac{2M_{\tilde{\chi}_3^0}^2}{(M_{\tilde{\chi}_3^0}^2 + M_Z^2 - M_{\tilde{\chi}_1^0}^2)}} \tag{2}$$

5 Hadronic Z^0 Reconstruction Analysis

The branching ratios relevant to this particular signal ($e^+e^- \rightarrow \widetilde{\chi}_3^0\widetilde{\chi}_4^0$) can be seen in Table 4 below. The cross section of this signal at 750 GeV is 22.8 fB[8]. With a beam luminosity of 500 fb^{-1}, $500 * 22.8 = 11400$ events are produced in a single year of data.

Resolving the box energy distribution of the Z^0 produced by the $\widetilde{\chi}_3^0$ was the focus of this analysis. In the early stages of this research, resolving the energy box of the Z^0 from the $\widetilde{\chi}_4^0$ was investigated. This would have been a very efficient way to measure the $\widetilde{\chi}_4^0$ mass. As can be seen in Table 4 though, the number of Z^0 events produced down this channel is significantly less than in the $\widetilde{\chi}_3^0$ case, and a box distribution could not be resolved even over $\widetilde{\chi}_3^0$ $\widetilde{\chi}_4^0$ events alone.

$\widetilde{\chi}_3^0$ branching ratios

decay channel	fraction
$\widetilde{\chi}_1^+W^-$	29.8
$\widetilde{\chi}_1^-W^+$	29.8
$\widetilde{\chi}_2^0Z^0$	21.4
$\widetilde{\chi}_1^0Z^0$	10.9
$\widetilde{\chi}_1^0h^0$	1.99
$\widetilde{\chi}_2^0h^0$	1.15

$\widetilde{\chi}_4^0$ branching ratios

decay channel	fraction
$\widetilde{\chi}_1^+W^-$	26.2
$\widetilde{\chi}_1^-W^+$	26.2
$\widetilde{\chi}_2^0h^0$	13.1
$\widetilde{\chi}_1^0h^0$	6.4
$\widetilde{\nu}_\tau\bar{\nu_\tau}$	2.51
$\overline{\widetilde{\nu}}_\tau\nu_\tau$	2.51
$\widetilde{\nu}_\mu\bar{\nu_\mu}$	2.5
$\overline{\widetilde{\nu}}_e\nu_e$	2.5
$\overline{\widetilde{\nu}}_\mu\nu_\mu$	2.5
$\widetilde{\nu}_e\bar{\nu_e}$	2.5
$\widetilde{\chi}_1^0Z^0$	2.06
$\widetilde{\chi}_2^0Z^0$	1.89

Table 4: $\widetilde{\chi}_3^0$ and $\widetilde{\chi}_4^0$ branching ratios. Blue decay channels are those that were focused on.

M_Z is about 91 GeV/c^2, so in the eyes of the detector, the Z^0 is unstable. The only way to see its energy distribution is to reconstruct it from its decay products. In attempting to isolate the Z^0 energy box, numerous decay modes were tried. The reaction mode that this analysis focuses on is shown in Figure 5. The decay channels shown in Figure 5 yielded the greatest statistics.

[8]This is with an electron polarization of 80% left

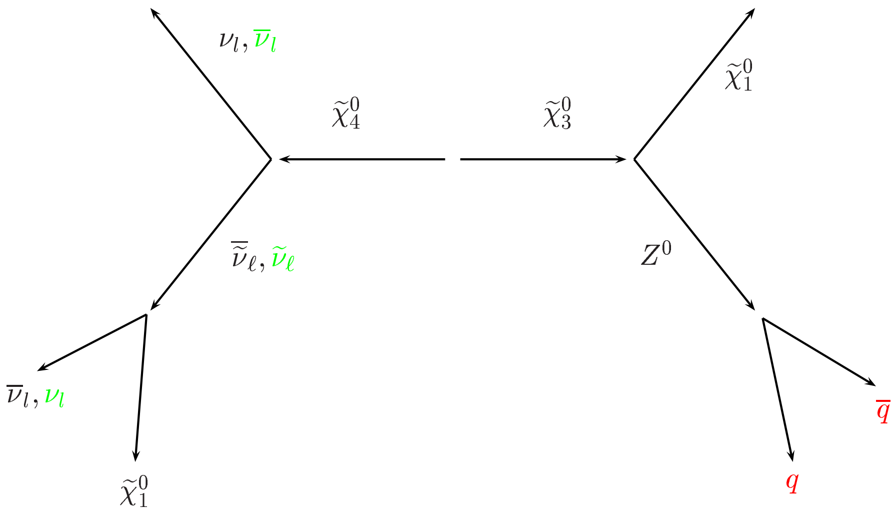

Figure 5: Decay Modes for the $\widetilde{\chi}_3^0$ and $\widetilde{\chi}_4^0$ investigated here. The red particles indicate the decay branches that yield visible particles. Green particles indicate the conjugate decays of those in black.

Z^0 Decay Mode	Branching Ratio
e^+e^-	3.37%
$\mu^+\mu^-$	3.37%
$\tau^+\tau^-$	3.37%
hadrons	68.9%
invisible	20.0%

Table 5: Z^0 Branching ratios.

The only visible particles in this reaction will be the decay products of the Z^0. The other side of the reaction, decay products coming from the $\widetilde{\chi}_4^0$, are all invisible to the detector[9]. Figure 5 shows the Z^0 decays into a quark anti-quark pair, but these quarks will not be seen in the detector. In fact, a free quark has never been seen in nature. The Strong force's potential contains a term that acts proportionally with distance, and so as one lone quark

[9]Sneutrinos decay into a neutrino and a $\widetilde{\chi}_1^0$ about 90% of the time for each of the three lepton flavors. Neutrinos and $\widetilde{\chi}_1^0$s interact only weakly with matter, so they are effectively invisible.

escapes from others, this potential blows up. If there is enough energy for these quarks to be pushed far enough apart, these quarks undergo a process called hadronization, and take shape into new particles call hadrons[10]. The Z^0 decays as seen in Table 5. From this table, it is clear that the hadronic decay mode is very prominent for the Z^0.

The main approach used for finding the events in Figure 5 was to look through all of the events in the data set, and find those where all of the visible particles in that event have an effective mass $\sim 91\ GeV/c^2$ (M_Z). In the ideal case, this signifies that a Z^0 is in that event and that no other visible particles besides those coming from the Z^0 are present. The formula that governs this approach is the relativistic energy equation shown below with the summation i's running over all of the visible particles in any event.

$$M = \sqrt{(\sum E_i)^2 - (\sum \overrightarrow{P_i} \cdot \sum \overrightarrow{P_i})} \tag{3}$$

Figure 6 shows the Z^0 mass resonance clearly.[11] When this same analysis was performed on all of the SUSY events produced, however, the Z^0 peak statistically became a small hump (Figure 7).

Comparing these two histograms indicated that there were many SUSY background processes in Figure 7 that needed to filtered out before something closer to Figure 6 was seen. To do this, a serious of cuts were devised that eliminated significant portions of this background while keeping as much signal intact as possible.

5.1 Cut on Events with a Lepton

The first was a cut on all events with a stable lepton ($e^{\pm}, \mu^{\pm}$) in them. The motivation behind this cut was to eliminate some of the more significant background processes, like selectron events ($e^+e^- \rightarrow \tilde{e}_L^+\tilde{e}_L^-$) and smuon events ($e^+e^- \rightarrow \tilde{\mu}_L^+\tilde{\mu}_L^-$) that are primarily leptonic in nature. Additionally, this cut tossed out many other of the less prominent leptonic decay processes[12].

[10] Hadrons can be bosons or fermions. Mesons are hadronic bosons, and are made from quark-antiquark pairs. Baryons are hadronic fermions made from three quarks.

[11] Note that Figures 6 and 7 also include leptonic Z^0 decays.

[12] $e^+e^- \rightarrow \tilde{\nu}_e\overline{\tilde{\nu}}_e$ is a prime example here. While the electron sneutrino decays to $\tilde{\chi}_1^+e^-$ only 9% of the time, the cross-section for this process is an order of magnitude larger than any other processes. Thus, the sneutrino signal is a dominant SUSY signal at this energy even though it's leptonic channel isn't. Many electron sneutrino events were cut here.

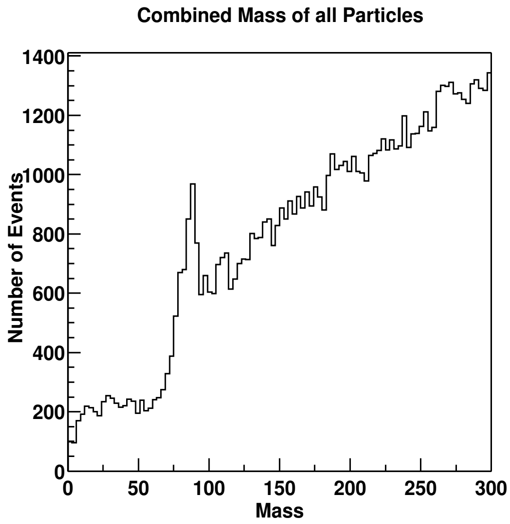

Figure 6: Effective mass of all visible particles for 10 years worth of signal only data.

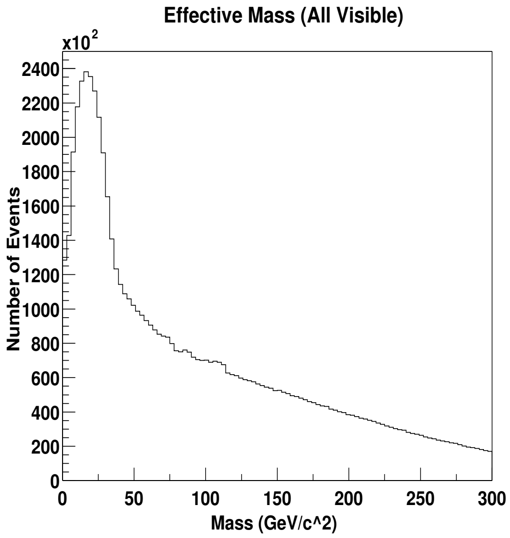

Figure 7: Effective mass of all visible particles for 10 years of all Supersymmetric processes.

This cut eliminated signal events that decayed down the three leptonic channels of the Z^0 decays (Table 5), as well as some hadronic decay events. This is an acceptable loss, as these lepton channels would have been swarmed by the very background events that this cut removed. As well, the hadronic channels yielded many more events, so this cut didn't effect the statistics too heavily. The effective mass plot after this cut can be seen in Figure 8. Table 7 shows the exceptional efficiency of this cut. This cut retained 73% of the initial hadronic signal events while removing 89% of the SUSY background events.

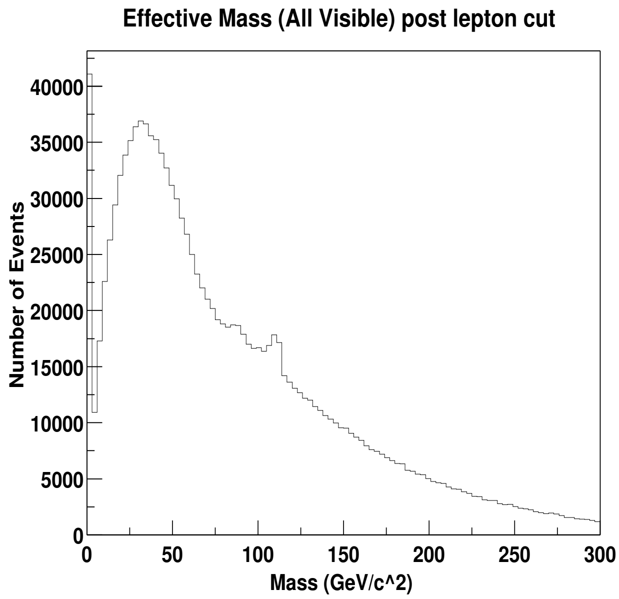

Figure 8: Effective Mass after the lepton cut.

After this cut, the hump around 91 GeV/c^2 was more visible. As seen, there is also a second hump at about 113 GeV/c^2 that becomes visible. This hump corresponds to events with a h^0 ($M_{h^0} = 113.97\ GeV/c^2$) and nothing else visible. The signal studied here contributes events to this hump from alternate decay channels, and so do the $\tilde{\chi}_2^0\tilde{\chi}_3^0$, $\tilde{\chi}_1^0\tilde{\chi}_3^0$, $\tilde{\chi}_2^0\tilde{\chi}_4^0$, and $\tilde{\chi}_1^0\tilde{\chi}_4^0$ SUSY signals. The greatest contributor here, however, is h^0Z^0 events with the Z^0 decaying down the two neutrino decay channels (Table 5 lists these decay channels as invisible).

5.2 τ Vertex Cut

As discussed in Section 3.2, the Vertex Detector portion of the NLC allows researchers to identify vertices that are apart from the main one. This second cut utilized the technique of reconstructing τ vertices. Reconstructing τ vertices is a technique that has been used frequently in the past with high efficiencies. There are many methods used in a full detector simulation that allow a researcher to identify a particular vertex as coming from a τ. In the software that was used in this study, these methods were not available. So a method was devised to simulate the certain percentage of events that can be resolved in the detector.

If there is a τ in one of the events, the distance that it traveled was calculated randomly based on the τ's known mean lifetime and its velocity. Then, founded on the numbers from previous and working detectors[9], a spatial resolution of 20 μm was assumed for the the Vertex Detector in the NLC [13]. After assuming this resolution, if a τ traveled a distance greater than 20 μm in the Vertex Detector, it could be identified, and that event could be cut.

A more thorough understanding of this cut can be detailed looking at the mathematical model used. All particle decays can be physically modeled using decaying exponentials. In this case, we can use the following expression to tell us how many particles there are left at any point x:

$$N(x) = N_0 e^{\frac{-x}{x_0}} \tag{4}$$

Here x_0 is a mean distance that is particular to each τ. x_0 is given by:

$$x_0 = (time)(velocity) = (\gamma\tau)(\beta c) = (\gamma\beta)(\tau c) = \frac{P_\tau}{M_\tau}\tau c$$

$\gamma\tau$ is the time with relativistic time dilation effects taken into account, and βc is the velocity of the τ by definition. The last step above comes from substitutions of the relativistic energy and momentum equations. So, x_0 is dependent on the momentum of the particular τ and two quantities that are known and common to every τ, $M_\tau = 1777 MeV/c^2$ and the mean decay lifetime multiplied by c, $\tau c = 87.11 \mu m$.

[13] 20 μm is actually a high estimate from the numbers in these references. It is commonly thought that the NLC will also most likely have a much better spatial resolution than machines currently in use.

Now, we can take this exponential expression and normalize it to a region (in this case $0 \to \infty$). We then arrive at the following expression:

$$R = \int_0^x \frac{1}{x_0} e^{\frac{-x}{x_0}} dx$$

If we choose R to be a probability, or in this specific case a random number between 0 and 1, then this random number R will correspond to an x that depends directly on the exponential function and the normalization constant. Knowing this, we can solve the above equation for x and get:

$$x = -x_0 ln(1 - R) \tag{5}$$

Now, using a random number and the momentum of any particular τ, we can generate the decay length of that particular τ based on the general probability of any decay length and that τ's momentum. We can see the effective mass distribution after cutting all events with a τ that has a longer decay length than 20 μm in Figure 9.

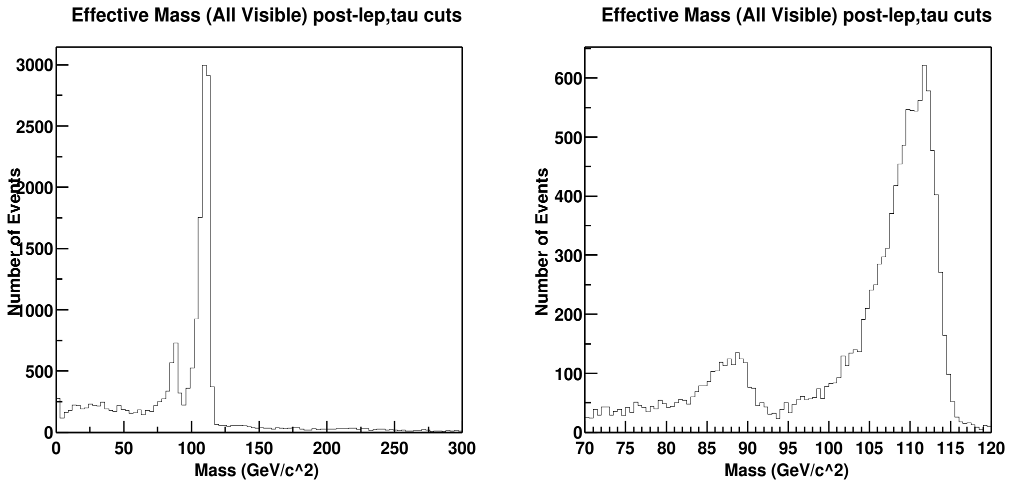

Figure 9: Effective Mass after the lepton cut and τ vertex cut, the right plot is the area of interest zoomed in.

5.3 Z^0 Mass Cut

The next step was to cut around the Z^0 mass peak in Figure 9 and plot the visible energy of the event. Table 7 shows the efficiency of this mass cut. For the results in Figure 9, cut limits at 83.0 and 93.0 GeV/c^2 were taken. As you can see in Figure 9 though, some portion of the Z^0 mass peak's low energy tail was cut. Decreasing this lower cut limit yields more background events per signal event. Cutting at the values above yielded the best signal to background ratio, and the cleanest box distribution.

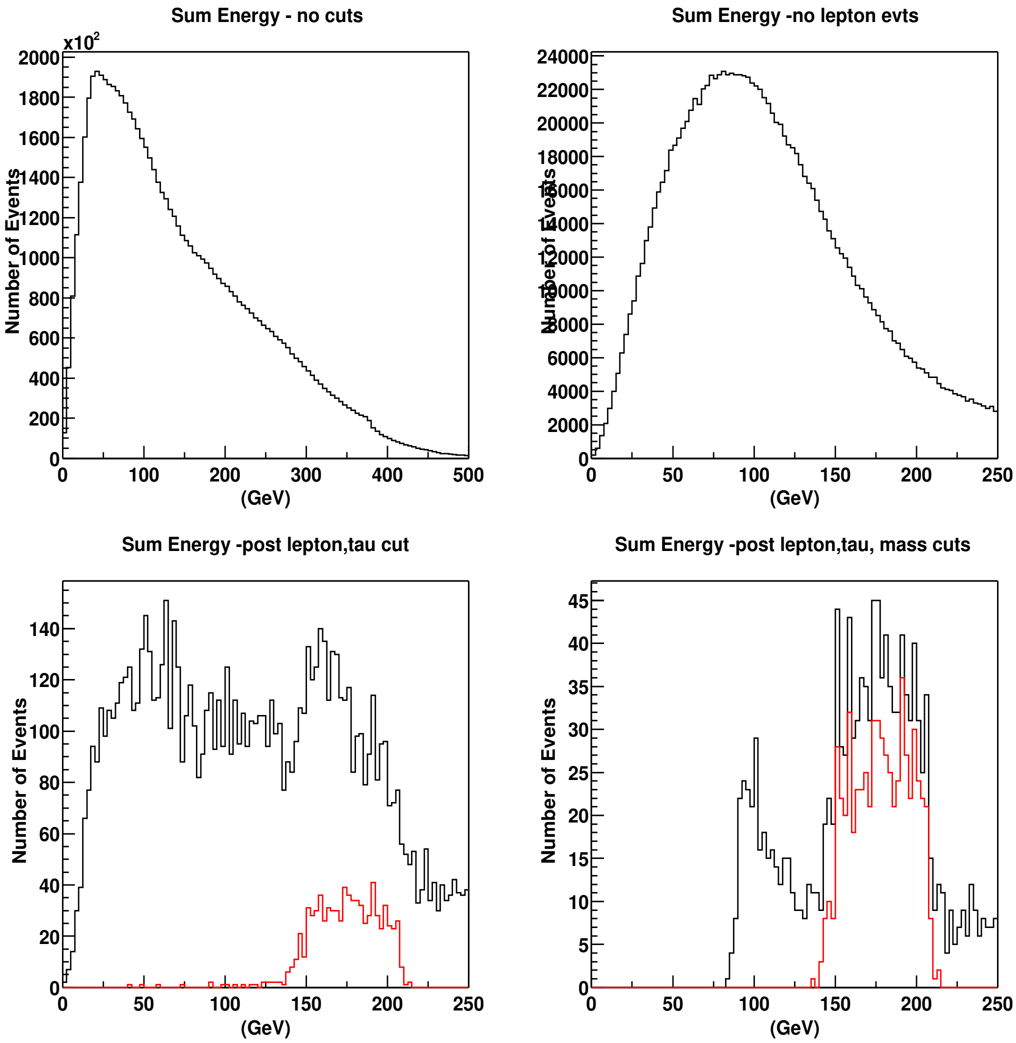

Figure 10: Summed energy of the events after and before each of the cuts outlined above. The upper left plot is before all cuts. The upper right plot is after the lepton cut. The lower left plot is after the lepton and tau cuts, and the lower right plot is after all of the cuts. The red is the signal that I am looking for and the black is the total distribution seen.

Figure 10 shows the total event energy distributions step by step through all of the cuts. The edges of the energy distribution in Figure 11 have been

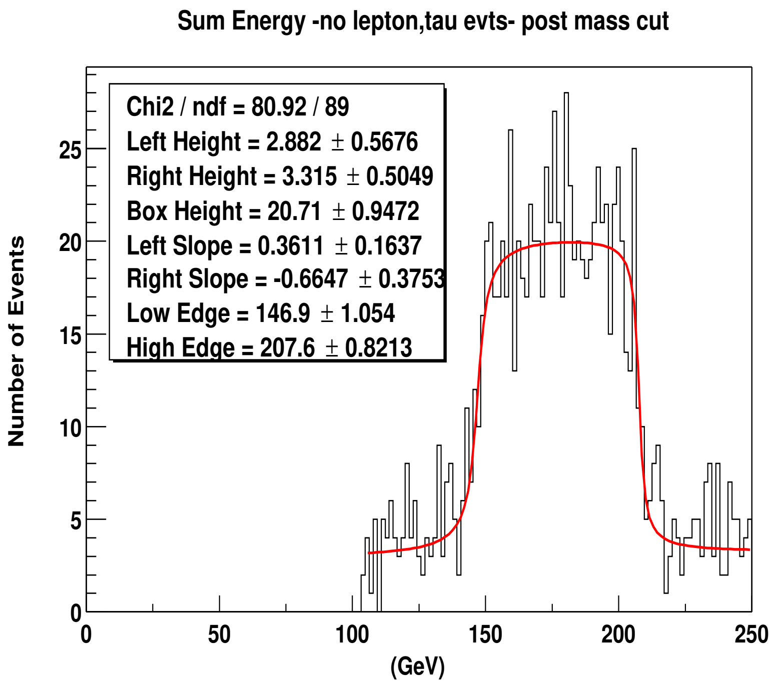

Figure 11: The results of applying a least squares fit to the energy after all of the cuts.

Particle	Input Mass	Calc Mass	Disc.
$\tilde{\chi}_3^0$	358.81	350 ± 2	2.5%
$\tilde{\chi}_4^0$	377.81	386 ± 3	2.1%

Table 6: Final Measured Masses of the $\tilde{\chi}_3^0$ and $\tilde{\chi}_4^0$ in GeV/c^2.

measured with a least squares fit. The lower right plot in Figure 10 is the same as Figure 11 but with different mass cutting limits. Figure 10's lower right plot lets in a significant portion of low mass tail discussed above.

The measured values of the edges in Figure 11 were then plugged into Equations 1 and 2. Table 6 shows a summary of the final results. The fit uncertainty of the edges was propagated through in quadrature for both measured masses. An uncertainty on the order of .1 GeV resolution in the $\tilde{\chi}_1^0$ mass was assumed based on a study conducted in our group [7]. The uncertainty on the measured mass of the $\tilde{\chi}_4^0$ was additionally dependent on the $\tilde{\chi}_3^0$ measurement error. The result is that the $\tilde{\chi}_4^0$ uncertainty is slightly larger.

Cut	# Signal Evts.	# Background Evts.	Total % Signal Retained
Initial	1064	12,360,022	N/A
Lepton	777	1,348,715	73%
Tau	769	41,199	72%
Mass	613	1,135	58%

Table 7: Cut efficiencies with respect to the initial number of signal events.

6 Conclusion

I was able to effectively measure the masses of both the $\tilde{\chi}_3^0$ and the $\tilde{\chi}_4^0$ given two main assumptions. First, that the mass of the $\tilde{\chi}_1^0$ has already been measured, and second, that the NLC has a Vertex Detector with a sufficiently good spatial resolution. In the case of this study, I assumed a resolution of 20 μm, but the cut that I used is robust around small alterations in this value.

The uncertainties on the measured masses versus the discrepancies on them is an area of continued research. My adviser and I have discussed these results, and it seems that it has been a reoccurring phenomenon with work conducted in this research group to have resolutions significantly smaller than discrepancies. The best response I can make to it at this time is that it is an issue that will receive further attention.

For the necessary statistics, and because the efficiencies of Supersymmetry investigations like this one are relatively low, I was forced to analyze 10 years of data. This restriction puts the study of this signal even further back on the time-line of SUSY signals to be studied.

This analysis in its current form lacks one significant aspect. The inclusion of the Standard Model events as further masking processes is important to this study. As an investigation of the feasibility of measuring these SUSY particles at the NLC, all processes that will occur at the NLC should be included. Unfortunately for the purposes of this thesis, I am currently in the middle of this investigation. So, while it will be done, it was not for this paper.

I would like to thank my advisor, Prf. Uriel Nauenberg, for his guidance, suggestions, and help in this work.

A The Next Linear Collider

A general schematic for the proposed next linear collider is shown below.

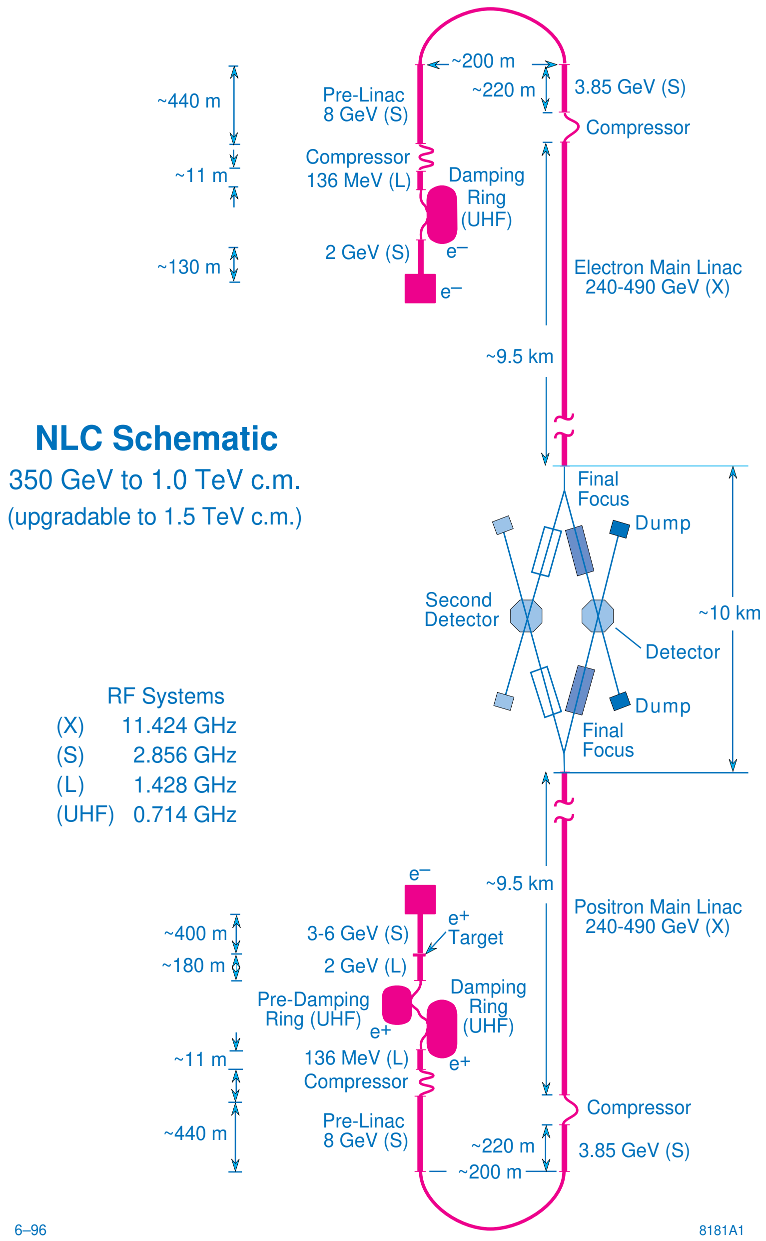

B Mass Derivation for an Asymmetric Reaction Mode

Mass derivations based on energy endpoints have been done before[6][7][11]. Tsukamoto et al. [6] is responsible for originating the methods used here, and I have used some similar techniques as those used in [7]. However, none of these previous studies address an asymmetric decay mode with only two visible energy endpoints, as in the case of the $\widetilde{\chi}_3^0\, \widetilde{\chi}_4^0$ signal. This asymmetry and sparsity of measurable quantities introduces a number of complications. For example, the $\widetilde{\chi}_3^0$ and $\widetilde{\chi}_4^0$ Lorentz boosts out of the electron-positron interaction center of mass frame are co-dependent with respect to energy and mass. In the end, though, there are two measurable quantities and two unknown quantities, so this system should be and is solvable.

The general schematic for what I am solving is:

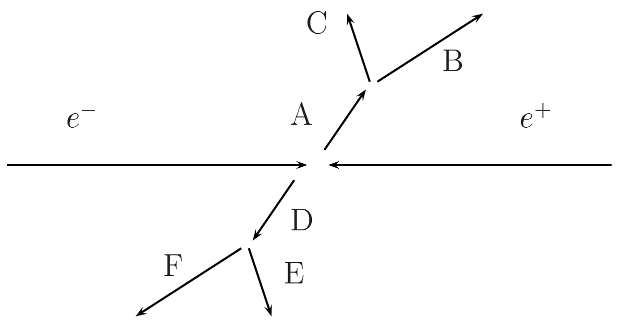

The purpose of these derivations is to find an expression for the mass of particles A and D dependent only on the energy endpoints of particle C and the masses of particles B and C. I am going to first derive an expression for γ_A that depends on the mass of both particles A and D. For the purpose of brevity and clarity, I will set $c = 1$ throughout these derivations and I will assume a few expressions that are straight-forward to derive. In the CM frame for the electron-positron collision, with $\sqrt{s}$ as the interaction energy of the accelerator, we can write the following[14]:

$$E_{CM} = \sqrt{s} = E_A^{CM} + E_D^{CM}$$

[14] A note with respect to the notation that I will use: As super- and sub- scripts CM and LAB will refer to the Center of Mass and Lab frames respectively.

$$= E_A^{CM} + \sqrt{M_D^2 + (P_D^{CM})^2}$$
$$= E_A^{CM} + \sqrt{M_D^2 + (P_A^{CM})^2}$$
$$= E_A^{CM} + \sqrt{M_D^2 + (E_A^{CM})^2 - M_A^2}$$

Where in these equations I have used the relativistic equation, $E^2 = P^2 + M^2$, and the fact that the A and D particles have equal and opposite momentum in this CM frame from momentum conservation. So now,

$$(\sqrt{s} - E_A^{CM})^2 = M_D^2 + (E_A^{CM})^2 - M_A^2$$

And multiplying through, we get:

$$(\sqrt{s})^2 - 2\sqrt{s}E_A^{CM} + (E_A^{CM})^2 = M_D^2 + (E_A^{CM})^2 - M_A^2$$

With the following expression that is derivable from relativistic energy and momentum definitions,

$$\gamma_A = \frac{E_A^{CM}}{M_A}$$

We can reduce the above to:

$$2\sqrt{s}\gamma_A M_A = M_A^2 - M_D^2 + \sqrt{s}^2$$

Or,

$$\gamma_A = \frac{\sqrt{s}}{2M_A} + \frac{(M_A^2 - M_D^2)}{2\sqrt{s}M_A} \tag{6}$$

Next I'll need an expression for the energy of particle C in the CM frame of A. In that frame we have:

$$E_B^{CM} = E_A^{CM} - E_C^{CM}$$

And squaring:

$$(E_B^{CM})^2 = (E_A^{CM})^2 + (E_C^{CM})^2 - 2E_A^{CM}E_C^{CM}$$

I'm now going to use the fact that P_A is zero in the CM frame of particle A, which implies that $E_A^{CM} = M_A$ and that $(P_B^{CM})^2 = (P_C^{CM})^2$. So,

$$M_B^2 = M_A^2 + M_C^2 - 2M_A E_C^{CM}$$

Or,

$$E_C^{CM} = \frac{M_A^2 + M_C^2 - M_B^2}{2M_A} \tag{7}$$

Now, we have the following expression for the energy and momentum of particle C with respect to the Lorentz boost of particle A:

$$E_C^{LAB} = \gamma_A(E_C^{CM} + \beta_A P_C^{CM} cos\theta)$$

This is the cosine expression which gives rise to the two endpoints. I will call the endpoints E^{HI} and E^{LOW} and drop the LAB notation assuming it from here on. The terms I get are:

$$E_C^{HI} = \gamma_A(E_C^{CM} + \beta_A P_C^{CM}) \tag{8}$$

$$E_C^{LOW} = \gamma_A(E_C^{CM} - \beta_A P_C^{CM}) \tag{9}$$

Adding and multiplying Equations 8 and 9 above, we can form two very useful expressions:

$$E_C^{HI} + E_C^{LOW} = 2\gamma_A E_C^{CM} \tag{10}$$

$$E_C^{HI} E_C^{LOW} = {\gamma_A}^2 (E_C^{CM})^2 - {\gamma_A}^2 {\beta_A}^2 (P_C^{CM})^2 \tag{11}$$

We should simplify Equation 11 a bit before we use it. I want first, though, to derive a basic relation between β_A and γ_A that will make this simplification process run smoother. The standard definition of γ_A is given as:

$$\gamma_A = \frac{1}{\sqrt{1-\beta_A^2}}$$

Squaring, we can get:

$$1 - \beta_A^2 = \frac{1}{\gamma_A^2}$$

And rearranging:

$$\beta_A^2 = 1 - \frac{1}{\gamma_A^2} = \frac{(\gamma_A^2 - 1)}{\gamma_A^2} \tag{12}$$

Now, to simplify Equation 11:

$$\begin{aligned}
E_C^{HI} E_C^{LOW} &= \gamma_A{}^2[(E_C^{CM})^2 - \beta_A{}^2(P_C^{CM})^2] \\
&= \gamma_A{}^2[(E_C^{CM})^2 - \beta_A{}^2(E_C^{CM})^2 + \beta_A{}^2 M_C^2] \\
&= \gamma_A{}^2[(1 - \beta_A{}^2)(E_C^{CM})^2 + \beta_A{}^2 M_C^2] \\
&= (E_C^{CM})^2 + \gamma_A{}^2 \beta_A{}^2 M_C^2
\end{aligned}$$

And now, substituting in Equation 12:

$$E_C^{HI} E_C^{LOW} = (E_C^{CM})^2 + (\gamma_A^2 - 1) M_C^2 \tag{13}$$

We can now solve Equation 10 above for γ_A and substitute this into Equation 13. Doing this will effectively eliminating all of the M_D dependence in Equation 13 and allow us to move significantly closer to solving this equation for M_A. So, rearranging Equation 10 we get:

$$\gamma_A = \frac{E_C^{HI} + E_C^{LOW}}{2 E_C^{CM}} \tag{14}$$

So now plugging this expression into Equation 13 we get the following:

$$E_C^{HI} E_C^{LOW} = (E_C^{CM})^2 + [\tfrac{E_C^{HI} + E_C^{LOW}}{2 E_C^{CM}}]^2 M_C^2 - M_C^2$$

And we can multiply through by $(E_C^{CM})^2$ to get a quartic expression in E_C^{CM}. We get:

$$(E_C^{CM})^4 - [E_C^{HI} E_C^{LOW} + M_C^2](E_C^{CM})^2 + (\frac{E_C^{HI} + E_C^{LOW}}{2})^2 M_C^2 = 0 \tag{15}$$

Now we can solve Equation 15 in terms of the general quartic $ax^4 - bx^2 + c = 0$ with:

$$a = 1$$
$$b = E_C^{HI} E_C^{LOW} + M_C^2$$
$$c = (\frac{E_C^{HI} + E_C^{LOW}}{2})^2 M_C^2$$

The general solutions are of the form:

$$x = -\sqrt{\frac{b}{2a} \pm \frac{\sqrt{b^2-4ac}}{2a}} \text{ and } x = +\sqrt{\frac{b}{2a} \pm \frac{\sqrt{b^2-4ac}}{2a}}$$

The two negative solutions are not physical solutions in this case, the center of mass energy of particle C cannot be negative. Additionally, of the two positive solutions remaining, I am going to take the positive solution based on the final numbers. So, now I'll set the above correct solution for x arbitrarily equal to a constant d, and continue. We know now from Equation 7 that:

$$E_C^{CM} = d = \frac{M_A^2 + M_C^2 - M_B^2}{2M_A}$$

Multiplying through by $2M_A$ and moving around a little, we can get a quadratic in terms of M_A:

$$M_A^2 - 2dM_A + (M_A^2 - M_B^2) = 0 \tag{16}$$

The solutions to this expression are given as:

$$M_A = \frac{2d \pm \sqrt{(2d)^2 - 4(M_C^2 - M_B^2)}}{2}$$

I am going to take the positive solution based on the kinematics of the event. So now, plugging all the values back in we get:

$$M_A = d + \sqrt{d^2 - ({M_C}^2 - {M_B}^2)} \tag{17}$$

with

$$d = \sqrt{\frac{(E_Z^{HI} E_Z^{LOW} + M_C^2)}{2} + \frac{\sqrt{(E_Z^{HI} E_Z^{LOW} + M_C^2)^2 - {M_C}^2 (E_Z^{HI} + E_Z^{LOW})^2}}{2}} \tag{18}$$

And going back to Equation 6, we can plug in the expression just derived for M_A into Equation 6 to solve it for the M_D. When we do this, skipping a few minor algebra steps, we get the following:

$$M_D = \sqrt{M_A^2 + \sqrt{s}^2 - \sqrt{s}(E_Z^{HI} + E_Z^{LOW})\frac{2M_A^2}{(M_A^2 + M_C^2 - M_B^2)}} \tag{19}$$

References

Note: All the papers with CU-HEP numbers can be found on the web at: http://hep-www.colorado.edu/SUSY/.

[1] Langacker, Paul and Nir Polonsky. "Uncertainties in Coupling Constant Unification." Physical Review D 47:9, (1993).

[2] Martin, Stephen P. "A Supersymmetry Primer." *Perspectives on Supersymmetry.* Ed. Gordon L. Kane. New Jersey: World Scientific Publishing Co. Pte. Ltd., 1998.

[3] Barron, James S. "The Capabilities of a Low Angle Cerenkov Detector for the NLC in the Midst of a Magnetic Field of 4 Tesla." September, 2000. COLO-HEP 449.

[4] Takeuchi, Christopher S. and Rory C. Kelly. "Feasibility Study of a Low Angle Cerenkov Detector." November, 1999. COLO-HEP 450.

[5] Paige, F., and S. Protopopescu, in *Supercollider Physics* p.41, edited by D. Soper (World Scientific, 1986); H. Baer, F. Paige, S. Protopopescu, and X. Tata in *Proceedings of the Workshop on Physics at Current Accelerators and Supercolliders,*, edited by J. Hewett, A. White, and D. Zeppenfeld (Argonne National Laboratory, 1993).

[6] Tsukamoto, Toshifumi *et al.*. "Precision Study of Supersymmetry at Future Linear e^+e^- Colliders." Physical Review D51 7, (1995).

[7] Dima, Mihai *et al.*. "Mass Determination Method for $\widetilde{e}_{L,R}$ Above Production Threshold" Physical Review D65, (2002).

[8] Allanach, B. C. *et al.*. "The Snowmass Points and Slopes: Benchmarks for SUSY Searches." European Phys. J. C25 113, (2002).

[9] The BaBar Collaboration. "The BaBar Detector" Nuclear Instruments and Methods in Physics Research. 479 1 (2002).

[10] Goodman, Elizabeth "The Search for the Supersymmetric Selectron." April, 1998. COLO-HEP 398.

[11] Williams, Brook. "Study of the Production of Supersymmetric Particles." April, 1998. COLO-HEP 402.